

Loop Closure from Two Views: Revisiting PGO for Scalable Trajectory Estimation through Monocular Priors

Tian Yi Lim^{1,*}, Boyang Sun^{1,*}, Marc Pollefeys^{1,2}, Hermann Blum^{1,3}

¹ ETH Zurich, ² Microsoft, ³ University of Bonn

* Equal contribution

Abstract—(Visual) Simultaneous Localization and Mapping (SLAM) remains a fundamental challenge in enabling autonomous systems to navigate and understand large-scale environments. Traditional SLAM approaches struggle to balance efficiency and accuracy, particularly in large-scale settings where extensive computational resources are required for scene reconstruction and Bundle Adjustment (BA). However, this scene reconstruction, in the form of sparse pointclouds of visual landmarks, is often only used within the SLAM system because navigation and planning methods require different map representations. In this work, we therefore investigate a more scalable Visual SLAM (VSLAM) approach without reconstruction, mainly based on approaches for two-view loop closures. By restricting the map to a sparse keyframed pose graph without dense geometry representations, our ‘2GO’ system achieves efficient optimization with competitive absolute trajectory accuracy. In particular, we find that recent advancements in image matching and monocular depth priors enable very accurate trajectory optimization from two-view edges. We conduct extensive experiments on diverse datasets, including large-scale scenarios, and provide a detailed analysis of the trade-offs between runtime, accuracy, and map size. Our results demonstrate that this streamlined approach supports real-time performance, scales well in map size and trajectory duration, and effectively broadens the capabilities of VSLAM for long-duration deployments to large environments.

I. INTRODUCTION

Simultaneous Localization and Mapping (SLAM) methods have become a cornerstone in any autonomous robotic system. A robust, accurate, and scalable SLAM solution is crucial for applications that require navigation over large-scale environments and/or long deployment times [1]. SLAM has been extensively studied over the past few decades [2–4], with methods deployed across various platforms in diverse environments for tasks such as robot navigation [5, 6], mixed reality [7, 8], autonomous driving [9, 10], and mobile device applications [11]. SLAM methods have become remarkably accurate even in very challenging environments [12], but achieving scalability remains challenging due to the substantial computational and storage demands involved. VSLAM methods are of particular interest due to the widespread availability and low cost of camera sensors, but in competitions such as the HILTI SLAM Challenge [13] they lag behind their LiDAR SLAM-based counterparts. In summary, despite a long line of research, a scalable and accurate solution to VSLAM is still missing.

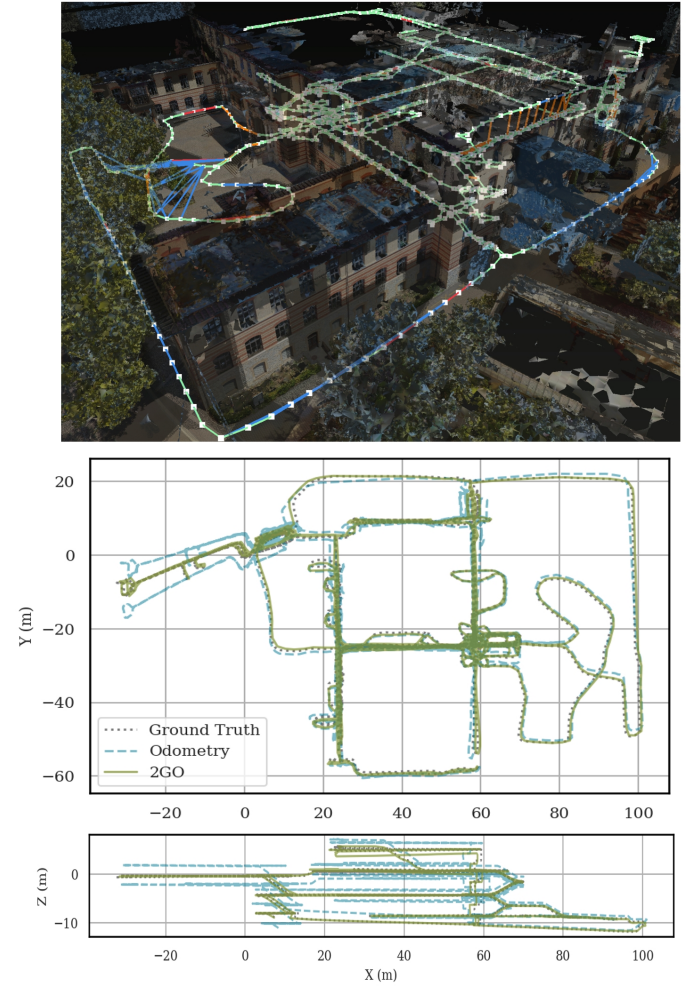


Fig. 1: **Top:** 2GO, our proposed system, refines a 1.1 h, 2.7 km trajectory collected from a quadrupedal robot, overlaid on a 3D reconstruction of the surroundings. Absolute and scale-free loop-closure edges are visible in yellow and blue, respectively. Loop-closure edges with both types of constraints present are in red. **Bottom:** It significantly improves the quality of the input trajectory, particularly in the Z-direction.

Recent advancements in VSLAM and VIO have primarily focused on improving accuracy and robustness. With accurate calibration, stereo visual odometry has even outperformed LiDAR-based methods on certain public benchmarks, such as KITTI [14]. Locally accurate odometry is becoming increas-

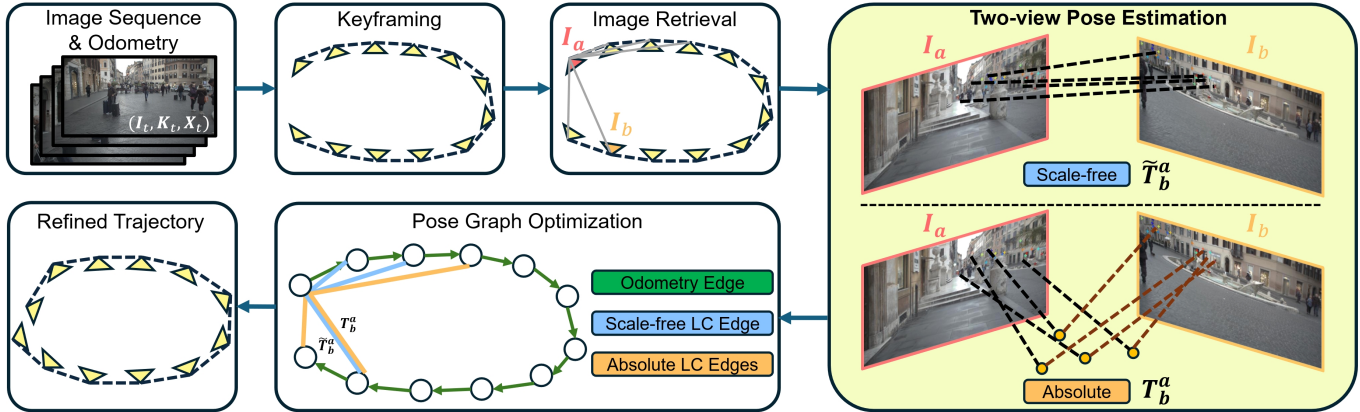


Fig. 2: **System Overview** From an input stream of odometry and images, we first downsample keyframes. Then we check for loop-closure candidates within previous keyframes and estimate the relative pose between candidate image pairs (metric and/or up-to-scale). Candidates are then filtered based on pose-estimation confidence and geometric checks and then added as two-view edges to the pose-graph map, which is optimized with PGO. Marked in yellow is the main innovation of this paper.

ingly available for visual-inertial setups [15, 16], and monocular odometry continues to make steady progress [17]. However, while visual odometry provides reliable local tracking, achieving globally accurate trajectory estimation requires loop closures and global optimization, where scalability remains a challenge. State-of-the-art methods rely on bundle adjustment (BA) to jointly optimize a globally consistent trajectory and reconstruction. The time complexity of BA is linear in the number of landmarks and cubic in the number of poses [18], making real-time performance difficult in large-scale scenes. Additionally, the sparse landmark point cloud generated during reconstruction is rarely utilized in downstream robotic modules. It is often too sparse for operator visualization, while planning methods typically require alternative data structures such as Truncated Signed Distance Fields (TSDF). In practice, fully-fledged mapping frameworks run separate processes to integrate a TSDF after optimizing the poses [19] or construct a mesh from the optimized landmark positions [20].

In this work, we explore a more scalable approach to VSLAM based on two key insights: (i) robust and **locally accurate odometry** is widely available on most robotic systems and other devices; (ii) large deep-learning models are increasingly improving at estimating geometry from single and multiple views, providing useful vision priors that enable the construction of **global relations** between keyframes without requiring a map. While the first development reduces the margin of improvement for BA given a trajectory from odometry, the second point raises the question whether optimization of a global geometric map is necessary at all. Therefore, we propose to optimize a globally consistent trajectory through pose-graph optimization (PGO), where loop-closure (LC) edges are constructed directly from pairs of keyframes. To this end, we revisit prior approaches for scale-free LC edges with modern image matchers and experiment with generating absolute LC constraints from metric monocular depth [21] or the MASt3R two-view estimator [22].

Our 2-view PGO approach, which we call ‘2GO’, therefore does not produce any 3D reconstruction. Instead, it leverages

locally accurate odometry for short-term consistency and vision priors to establish global relations between keyframes, enabling a fully map-free optimization through PGO. It constructs and optimizes only a pose graph with odometry edges, LC edges, and keyframes. Through extensive experiments on large-scale trajectories, we show that this simplification yields lower map size and runtime. Surprisingly, in most trajectories, 2GO also yields higher pose accuracy than SotA VSLAM methods. In summary, our contributions are:

- **2GO**, a two-view PGO framework that leverages the potential of recent advancements in monocular vision priors for large-scale VSLAM.
- An analysis of runtime, accuracy, and map size of VSLAM methods on long trajectories and large scenes.
- Comprehensive experiments on large-scale datasets, with different odometry sources, and comparisons with a mapping system that performs global BA.

II. RELATED WORK

A. Large-Scale SLAM

Conventional VSLAM and VIO approaches [15, 16, 23, 24] rely on building a metric 3D map and jointly optimizing the map and camera pose. They have demonstrated reliable performance across various public benchmarks [13, 25, 26]. These methods achieve high local accuracy, but often face scalability challenges. To improve the scalability of VSLAM, previous methods have explored reducing the computational cost of bundle adjustment by limiting it to a sliding window or running it at a low frequency [24, 27]. Some approaches eliminate BA entirely and rely solely on pose graph optimization, though they still require landmarks to establish loop closure constraints [15, 28]. Orthogonal to our work, prior research has focused on reducing the number of loop closures, as they are a primary cost factor in PGO [28, 29]. In contrast, our approach takes this further by not only skipping BA but also eliminating reconstruction and triangulation steps.

B. Vision-based Priors

Recent SLAM methods have explored monocular depth to enhance accuracy and robustness. Early approaches, such as [30], optimize camera poses and dense depth maps using a regularized energy function. More recent Neural-SLAM methods, including [31], leverage monocular depth estimators for dense reconstruction. Predicting geometric priors from monocular inputs, such as depth and surface normals [21, 32, 33], has made significant progress. However, these monocular priors remain underexplored in SLAM, particularly in sparse monocular settings. It remains unclear how to effectively use depth priors without performing dense reconstruction.

Beyond advances in monocular priors, two-view tasks have also seen significant progress, including feature matching [34–36], visual place recognition (VPR) [37, 38], and two-view reconstruction [22, 39]. Improvements in feature detectors and matchers have enabled robust 2D-2D matching in more challenging scenarios, such as wide-baseline settings. Global VPR methods have been widely explored and deployed in visual localization [40], with increasing attention on map-free localization due to their efficiency on edge devices, such as those used in augmented reality (AR) [41, 42]. For instance, *MARLoc* [43] integrates deep-learned 2D features and matchers with global image descriptors, achieving precise map-free localization on AR devices. A similar concept can be applied to SLAM to enhance loop-closure edge construction in a map-free manner. Two-view reconstruction priors have also been initially explored in both Structure-from-Motion(SfM) [44, 45] and VSLAM [46]. However, these methods still rely on reconstruction maps and perform dense bundle adjustment.

III. LOOP CLOSURES FROM TWO VIEWS

Figure 2 provides an overview of 2GO. To constrain a trajectory using loop closures without reconstructing the 3D geometry of the environment, the system first finds LC candidates via image retrieval from previous keyframes and then explores different options for establishing pose constraints between image pairs. Finally, pose graph optimization (PGO) is performed using the identified LC edges to refine the prior trajectory derived from odometry. In this section we introduce how we construct different variants of loop-closure edges from two views. In Section IV we describe how these two-view constraints are used in the proposed SLAM system.

A. Problem Statement

Given a sequence of images from a calibrated camera and their corresponding odometric poses, the input to 2GO at time t is a 3-tuple $(\mathcal{I}_t, \mathbf{X}_t, \mathbf{K}_t)$. $\mathcal{I}_t \in \mathbb{R}^{H \times W \times C}$ is the rectified image from the camera. $\mathbf{X}_t \in \text{SE}(3)$ is the pose of the camera with respect to a reference frame. And $\mathbf{K}_t \in \mathbb{R}^{3 \times 3}$ are the camera intrinsics. 2GO incrementally refines the overall trajectory up to the present timestamp N , $\hat{\mathcal{X}} = (\hat{\mathbf{X}}_1, \hat{\mathbf{X}}_2, \dots, \hat{\mathbf{X}}_N)$. Without loss of generality, we describe the following methodology for a single-camera system. However, the approach extends naturally to multiple cameras,

provided that the extrinsic transformations to the estimated odometry frame are known.

B. Image Retrieval

The image retrieval stage identifies LC candidates—image pairs that can establish two-view constraints by observing the same region of the environment. Given a new input keyframe \mathcal{I}_k , image retrieval searches previous keyframes $\mathcal{I}_{1,2,\dots,k-1}$ for LC candidates, according to their *appearance* and *geometric* similarity, analogous to the *long-term* and *mid-term* data associations described in [24]. Unlike conventional image retrieval methods for LC detection, 2GO prioritizes high recall over high precision, as multiple filtering stages (detailed in Section IV-C), mitigate outliers introduced during image retrieval. This aggressive strategy increases the likelihood of detecting valid LCs to refine the input trajectory.

Similarity LCs: 2GO leverages recent visual place priors to identify image pairs with visual similarity. Specifically, it employs a visual place recognition network, *BoQ* [47], to generate a global descriptor \mathbf{F}_t for each image \mathcal{I}_t . This approach is well-established in SfM methods [40], where image correspondences are retrieved from large collections of unordered images. However, only a few SLAM systems have integrated VPR [48]. The VPR model is trained to ensure that the descriptors of two images are close in a similarity metric $\langle \mathbf{F}_a, \mathbf{F}_b \rangle$ (in our case the dot product), if \mathcal{I}_a and \mathcal{I}_b share visual overlap. Hence, we define a set of similarity LCs, \mathcal{C}_{sim} for a given image \mathcal{I}_k by selecting the n_{sim} images with most similar descriptors:

$$\mathcal{C}_{k,\text{sim}} = \left\{ \mathcal{I}_j \mid j \in \text{Top}_{j=0 \dots k-1}^{n_{\text{sim}}} \langle \mathbf{F}_k, \mathbf{F}_j \rangle \right\} \quad (1)$$

where $\text{Top}_A^n(\cdot)$ picks the top n elements out of A according to the given metric.

Proximity LCs: We also consider candidate LCs based on the geometric difference between the current and previous keyframe poses. This allows retrieving images that might otherwise be missed due to low visual similarity, such as those affected by large viewpoint changes. Since the robust learned matchers [22, 49] used in the subsequent steps can establish correspondences even across wide baselines, incorporating such LC candidates is beneficial. To accomplish this, we first find the set of nearby previous keyframes:

$$\tilde{\mathcal{C}}_{k,\text{prox}} = \left\{ \mathcal{I}_j \mid \forall j : \text{Rot}(\hat{\mathbf{T}}_j^k) < \delta_r \wedge \text{Trans}(\hat{\mathbf{T}}_j^k) < \delta_t \right\} \quad (2)$$

where $\hat{\mathbf{T}}_j^k = \hat{\mathbf{X}}_k^{-1} \hat{\mathbf{X}}_j$ denotes the relative transform between the current estimate of the poses of keyframes i and j , and δ_r and δ_t are the thresholds for rotational and translational differences, respectively. We prioritize matches with a larger time gap $\Delta t(\mathcal{I}_k, \mathcal{I}_j)$ between images, as they are more effective in correcting odometry drift.:

$$\mathcal{C}_{k,\text{prox}} = \text{Top}_{\mathcal{I}_j \in \tilde{\mathcal{C}}_{k,\text{prox}}}^{n_{\text{prox}}} \Delta t(\mathcal{I}_k, \mathcal{I}_j) \quad (3)$$

Subsequently, LC candidates $\mathcal{C} = \mathcal{C}_{\text{sim}} \cup \mathcal{C}_{\text{prox}}$ are passed to the two-view pose estimation module.

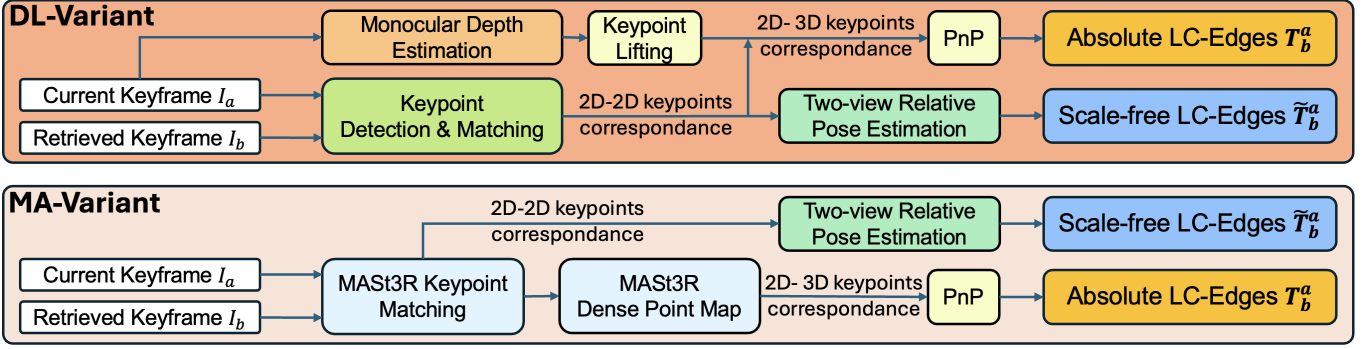


Fig. 3: **Two-view Pose Estimation** Both the DL and MA variant establish 2D-2D and 2D-3D feature correspondences for scale-free and absolute LC edges, respectively. The DL-variant employs separate deep learning models in a modular pipeline, while the MA-variant achieves this with a single two-view reconstruction model.

C. Constructing Two-View LC Edge

In conventional VSLAM and SfM methods, image poses are typically estimated via PnP using 2D-3D correspondences from an estimated metric map. Early Pose-SLAM approaches also relied on landmarks to define LC constraints without optimizing their positions [28]. 2GO eliminates the need for explicit 3D landmarks by (i) revisiting up-to-scale LC edges from 2D-2D matches and (ii) leveraging metric monocular depth prior for single-view 3D geometry estimation.

For each keyframe \mathcal{I}_k , 2GO estimates its relative pose $\mathbf{T}_a^k \in \text{SE}(3)$ to each LC candidate $\mathcal{I}_a \in \mathcal{C}$. Figure 3 illustrates two variants of this process for obtaining *scale-free* $\tilde{\mathbf{T}}_a^a$ and *absolute* \mathbf{T}_a^a two-view LC edges. The **DL-variant** follows conventional pipelines, using separate models for keypoint detection [50], matching [49], and keypoint depth estimation via metric monocular depth (MDE) [21]. In contrast, the **MA-variant** employs the MAS3R two-view model [22], which predicts 2D keypoint matches and 2D-3D correspondences through a single model.

Scale-free LC-Edge: The 2D keypoint correspondences between two images yield the essential matrix \mathbf{E} [51]. The up-to-scale relative pose between the two keyframes $\tilde{\mathbf{T}}_a^a = [\mathbf{R}_a^k \mid \tilde{\mathbf{t}}_a^a]$ can then be obtained by decomposing $\mathbf{E} = [\tilde{\mathbf{t}}_a^a] \times (\mathbf{R}_a^k)^T$. Similar as [52], the scale-free pose residual $\mathbf{r}_S(\tilde{\mathbf{T}}_b^a, \tilde{\mathbf{T}}_a^a)$ is computed as the pose error between a scale-free pose measurement $\tilde{\mathbf{T}}_b^a$ and the expected measurement $\hat{\mathbf{T}}_b^a$ from the current estimate in the pose graph.

$$\mathbf{r}_S(\hat{\mathbf{T}}_b^a, \tilde{\mathbf{T}}_b^a) = \begin{bmatrix} \tilde{\mathbf{t}}_b^a - \text{norm}(\hat{\mathbf{t}}_b^a) \\ \mathbf{R}_b^a \boxminus \hat{\mathbf{R}}_b^a \end{bmatrix} \in \mathbb{R}^6 \quad (4)$$

$$\text{norm}(\mathbf{t}) = \begin{cases} \frac{\mathbf{t}}{\|\mathbf{t}\|}, & \|\mathbf{t}\| > 0, \\ \mathbf{0}, & \|\mathbf{t}\| = 0. \end{cases} \quad (5)$$

Here, \boxminus denotes the operation mapping the difference in expected and measured rotations from the Lie Group $\text{SO}(3)$ to a vector in \mathbb{R}^3 for optimization [53]. In a scale-free pose measurement, the translation vector $\tilde{\mathbf{t}}_b^a$ is a unit vector. The expected translation $\hat{\mathbf{t}}_b^a$ is therefore also normalized before the two translation vectors are compared. The rare case $\|\tilde{\mathbf{t}}_b^a\| = 0$ is a pure rotation. To prevent numerical instabilities, these residuals are not included in the pose graph.

While scale-free LC-edges do not constrain the scale of the relative pose between two keyframes, they can still constrain the pose graph if enough scale-free edges are added. This is demonstrated in our experimental evaluations.

Absolute LC-Edge: In the DL-variant, a MDE model is used to obtain a metric depth map $\mathbf{D}_k \in \mathbb{R}^{H \times W}$ from \mathcal{I}_k . \mathbf{D}_k is used to lift the detected keypoints $\mathbf{p}_0^k, \dots, \mathbf{p}_N^k$ to 3D.

$$\mathbf{P}_i^k = d_i^k K_k^{-1} \begin{bmatrix} \mathbf{p}_i^k \\ 1 \end{bmatrix} \quad (6)$$

Here, d_i^k denotes the estimated depth value at the pixel \mathbf{p}_i^k .

In the MA-variant, MAS3R predicts a dense point-map $\mathbf{D}' \in \mathbb{R}^{H \times W \times 3}$, where each pixel in \mathcal{I}_k has a predicted position relative to \mathbf{X}_k . The coordinates of \mathbf{D}' indexed at $(u, v) = \mathbf{p}_i^k$, directly give \mathbf{P}_i^k .

Both two variants generate 3D-2D correspondences $(\mathbf{P}_i^k, \mathbf{p}_i^a)$ between \mathcal{I}_k and \mathcal{I}_a . These allow a PnP solver to obtain an absolute pose between them, yielding \mathbf{T}_a^k , which is incorporated into the pose graph as an absolute LC-Edge.

IV. SYSTEM IMPLEMENTATION

This section introduces how we build a complete trajectory estimation system around the two-view LC mechanism introduced in Section III. Given the raw input image and odometry streams, we subsample the camera stream into keyframes. During the image retrieval as introduced in Section III-B, we run filtering steps to rule out potential false-positive LCs. This loop is repeated for every new incoming keyframe and we construct the PGO that includes both filtered scale-free and absolute LC-edges to regularly optimize the trajectory.

A. Keyframing

2GO enforces spatial sparsity by choosing new keyframes solely based on the translational or rotational distance from the current frame to the previous keyframe, following a simplified subset of the rules from [19]. 2GO does not maintain a landmark map, making landmark triangulation between consecutive keyframes unnecessary. As a result, consecutive keyframes do not require a minimum number of covisible keypoints, allowing for a sparser selection strategy that enhances scalability. Furthermore, as relative poses between consecutive

frames can be obtained from input odometry, sophisticated keyframing strategies based on covisible keypoints [19] or difference in optical flow [54] are not necessary.

B. Two-View Pose Estimation

To compute relative pose between two LC frames constructed in Section III-C, 2GO uses the *COLMAP* [55] implementation of relative pose estimation. For generating keypoint correspondences between two images, the DL-Variant pipeline uses *DISK* features [50] and the *LightGlue* [49] matcher. We then estimate the metric depth through Metric3Dv2 [21]. The full set of hyperparameters is reported in the appendix Section C.

C. LC Filtering

Before integration into the pose graph, LC edges undergo feasibility filtering to enhance robustness against false positives in image retrieval:

Image Matching Feasibility: Scale-free and absolute LC-Edges require sufficient 2D-2D and 2D-3D correspondences, respectively. This filter uses the image matchers to ensure that images have enough meaningful visual overlap.

Geometric Feasibility: During computation of scale-free and absolute LC-Edges, the respective solvers assess whether the given correspondences yield a consistent model. This ensures the overall geometric consistency of the correspondences from image matching.

Pose-Graph Consistency: The computed transform between images should remain consistent with the current optimized trajectory. This enhances robustness against false-positive matches in visually similar environments.

D. Pose Graph Optimization

Optimizing the pose graph is analogous to solving a nonlinear least squares problem. The *iSAM2* incremental optimizer as implemented in *GTSAM* [56] is used as the back-end for optimization. In 2GO, the objective function of its PGO is formulated as:

$$\hat{\mathcal{X}} = \arg \min_{\mathcal{X}} \underbrace{\|\mathbf{r}_P(\mathcal{X}, \mathbf{X}_0)\|_{\Sigma_P}^2}_{\text{prior}} + \underbrace{\sum_{e \in \mathcal{O}} \|\mathbf{r}_A(h(\mathcal{X}), e)\|_{\Sigma_e}^2}_{\text{odometry edges}} + \underbrace{\sum_{l \in \mathcal{L}_a} \rho(\|\mathbf{r}_A(h(\mathcal{X}), l)\|_{\Sigma_{l_a}}^2)}_{\text{absolute LCs}} + \underbrace{\sum_{l \in \mathcal{L}_s} \rho(\|\mathbf{r}_S(h(\mathcal{X}), l)\|_{\Sigma_{l_s}}^2)}_{\text{scale-free LCs}} \quad (7)$$

where, $\|\mathbf{a}\|_{\Sigma}^2 = \mathbf{a}^T \Sigma \mathbf{a}$ denotes the L2 norm of $\mathbf{a} \in \mathbb{R}^n$ weighted by $\Sigma \in \mathbb{R}^{n \times n}$. $h(\mathcal{X})$ is the measurement function that obtains the relevant expected measurement from \mathcal{X} . $\rho(\cdot)$ denotes a robust Cauchy loss [57]. The overall error sums over odometry edges, absolute LC edges, and scale-free LC edges. Three types of residual are defined:

- $\mathbf{r}_A(\hat{\mathbf{T}}_b^a, \mathbf{T}_b^a) \in \mathbb{R}^6$, representing the pose error between an absolute pose measurement $\mathbf{T}_b^a \in \text{SE}(3)$ from frame b to a and its expected measurement $\hat{\mathbf{T}}_b^a \in \text{SE}(3)$ in the pose graph. This residual is well-studied and commonly used in PGO applications [15, 16, 20]. The difference in

expected and measured poses is mapped to a vector space \mathbb{R}^6 from $\text{SE}(3)$ for optimization [53].

- $\mathbf{r}_P(\mathcal{X}, \mathbf{X}_0) = \mathbf{r}_A(\hat{\mathbf{X}}_0, \mathbf{X}_0) \in \mathbb{R}^6$ represents a prior, anchoring the current estimate of the first pose $\hat{\mathbf{X}}_0$ to its initial value \mathbf{X}_0 .
- $\mathbf{r}_S(\hat{\mathbf{T}}_b^a, \mathbf{T}_b^a) \in \mathbb{R}^6$, is the pose error between a scale-free pose measurement $\hat{\mathbf{T}}_b^a$ and the expected measurement \mathbf{T}_b^a from the current estimate in the pose graph, as Equation (4) introduced in Section III-C.

PGO is performed every $\lfloor N/l \rfloor$ keyframes, where N is the total number of keyframes and l is a tunable parameter. This keeps optimization tractable as the pose graph grows denser.

V. EXPERIMENTS

A. Experiment Setup

2GO focuses on optimizing odometry in large-scale scenarios. To evaluate its performance, we conduct experiments using different odometry input sources across various datasets and benchmarks. Among the commonly used SLAM datasets, such as EuRoC [26], HILTI-22 [13], TUM-VI [58], and ETH3D-SLAM [59], KITTI offers the largest-scale trajectories with dense ground truth, making it a representative conventional benchmark. In addition to KITTI, we select the Vision Benchmark in Rome (VBR) [60], a recent dataset featuring long-duration, large-scale sequences. To further demonstrate 2GO’s real-world applicability, we evaluate it on a large-scale robot recording spanning approximately 1.1 h and 2.7 km.

For comparison we evaluate several odometry methods, some of which we also use to generate odometry inputs for 2GO. **VINS-Fusion** [15, 23] is a lightweight sliding-window VO/VIO system with a bag-of-words place recognition module that performs 4-DOF PGO on loop closure edges. **OpenVINS** [61] is an efficient filtering-based VIO system. **DPVO** [17] is a deep learning-based monocular visual odometry system. **ORB-SLAM3** [24] employs a sliding-window optimization approach in VSLAM and includes a bag-of-words place recognition module, performing map merging and BA when loop closures are detected. Additionally, We introduced the LiDAR odometry method **KISS-ICP** [62] to track challenging sequences.

We compare 2GO with the optimization backend of existing methods. **Kimera** [20, 54] is a SLAM system that fuses sliding-window VIO with external odometry while using a bag-of-words place recognition method and a robust 6-DOF PGO based on Graduated Non-Convexity (GNC) [63]. **Maplab2.0** [19] is a mapping framework capable of fusing multimodal sensor inputs. It uses covisible visual keypoints for place recognition and enforces global consistency by merging covisible keypoints between keyframes and performing global BA. We evaluate the variants with binary features (**BIN**) and with SuperPoint [64] (**SP**). **VINS-PGO** is the PGO backend of VINS-Fusion, which has a bag-of-words place recognition module that performs 4-DOF PGO on loop closure edges.

Unless specified otherwise, this section presents the DL variant results of 2GO, incorporating both scale-free and

absolute LC edges, with VINS-Fusion odometry as input. We showcase the several aspects of 2GO in separate experiments.

B. Is 2GO more scalable?

As 2GO aims to scale towards large-scale scenarios, we first evaluate its scalability. Table II shows the runtime and storage size evaluation results on the longest handheld VBR sequence, *spagna_train0*, with a distance of 1.56 km and a 1414s duration. 2GO only requires 82.5% of the real-time duration to process the entire input sequence. The only other method within real-time is Maplab-BIN, while Kimera and ORB-SLAM3 can be considered close to real-time. Two outliers are much slower: VINS-PGO takes $4.4 \times$ real-time to iteratively perform global PGO. VINS-PGO uses the same keyframing strategy for odometry and pose refinement, resulting in more than 10000 keyframes. In contrast, 2GO optimizes only 740 keyframes. Even though both methods do not perform BA, this illustrates the growing time complexity of PGO with the number of input poses. The second outlier is Maplab-SP that requires roughly $10 \times$ real-time to generate a map of camera poses and landmarks, as it uses the computationally expensive SuperPoint and SuperGlue models to detect and match keypoints between all pairs of consecutive frames. A detailed breakdown of 2GO’s runtime is in Appendix Section B.

We compare map sizes only between Maplab and 2GO, as VINS-PGO and Kimera lack functionality for saving maps. The Maplab map includes the pose graph, 3D landmark locations and descriptors, and keypoints coordinates in keyframes. Given that all other compared methods require this information and some additionally keep Bag-of-Words keyframe descriptors, this serves as a representative comparison between reconstruction-based and reconstruction-free map sizes. 2GO requires less than half of the storage of Maplab-BIN and roughly a quarter of Maplab-SP. However, none of the maps are prohibitively large.

This analysis confirms that our proposed approach effectively handles long trajectories. It remains one of the few methods within real-time constraints while maintaining the smallest map size among all baselines.

C. How do different LC edges contribute to the optimization?

We evaluate 2GO’s performance across DL and MA variants and different LC-edge combinations. Table I shows results on the *ciampino_train0* VBR sequence using KISS-ICP odometry, and the KITTI-00 sequence using VINS-Fusion odometry. Parameters for keyframing and image retrieval are held constant. We empirically tune the covariances before conducting experiments on our own collected data and keep them fixed over all experiments. We measure the accuracy of LC-Edges by comparing the estimated transformation between two keyframes k and a , \mathbf{T}_a^k with the relative transform between their ground-truth poses, \mathbf{X}_k^* and \mathbf{X}_a^* , computed as $\mathbf{X}_k^{*-1} \mathbf{X}_a^*$. The translation error for scale-free LC-edges is given as the

¹ORB-SLAM3 crashes when saving the map, requiring up to 28.8 GB RAM at the end of mapping, setting an upper bound on map size. As a lower bound, we use Maplab-BIN, which also stores 3D landmarks with binary descriptors.

angle between the normalized unit vectors $\tilde{\mathbf{t}}_a^k$ and $\text{norm}(\mathbf{t}_a^k)$. Here, the superscript “ $*$ ” denotes ground-truth.

All variants can run in (close-to) real time. DL scale-free is the only one not requiring MDE, and has thus lower runtime. The MASt3R model performs both keypoint matching and depth estimation in the same model, which means using only scale-free edges does not give a runtime advantage.

The DL-variant LCs are more accurate than MA for both scale-free and absolute LC-Edges. Impressively, DL-variant absolute LC-Edges obtain a median translation error of 0.25 m in the VBR sequence. However, our results also show that LC accuracy does not necessarily correlate with ATE of the trajectory, because it also depends on the number and distribution of LCs. The results further indicate that scale-free LC-Edges are effective in improving the trajectory. On the VBR sequence, both DL and MA variants utilizing only scale-free LC-Edges improve the RMSE ATE of the input competitively. While the MA variant using only scale-free LC-Edges is the best-performing method among MA variants for VBR, it does not help at all to get a good trajectory for KITTI-00, likely due to bad concentration of the edges in one part of the trajectory. This shows that two-view estimation is very dependent on model generalization, and each model performs differently on different domains. We can from the presented data not make out a clear best variant or model. Between the two sequences, the DL-Both variant yields the most consistently high improvement in ATE and finds more LCs, which is why we choose it for all other experiments.

D. How accurate is 2-View PGO?

We evaluate global trajectory error by comparing the RMSE Absolute Trajectory Error (ATE), computed using *evo* [65]. For most methods, ATE is computed after applying a 6-DOF Umeyama alignment [66] between the input and ground-truth trajectories. Results are shown in Table III. 2GO consistently improves the different input odometry in nearly all cases and often achieves the highest accuracy among the compared PGO and BA-based methods. VBR has longer and more challenging sequences as some VIO methods fail to track, or results in much higher error than on KITTI.

In cases such as *ciampino_train0* with ORB-SLAM3 or *spagna_train0* with VINS-Fusion, where the odometry deviates significantly at certain locations, 2GO is unable to fully recover these errors and may even produce less accurate trajectories than the input. Correcting severely incorrect odometry vertices using only LC edges in PGO is inherently challenging. On the other hand, odometry with a consistent drift, such as *ciampino_train0* with OpenVINS, can be significantly improved, as it lacks extreme local deviations. A visualization of this effect is provided in Appendix Figure 9 and Figure 10. This aligns with our assumption that the input odometry must be sufficiently accurate locally for 2GO to be effective. Notably, on the long trajectories of VBR, 2GO outperforms Kimera, VINS-PGO, and Maplab in refining the same input odometry. In contrast, on KITTI, most optimization methods yield reasonable outputs with some improvements

Dataset	2GO Variant	Median Trans. Err.	Median Rot. Err.	#LC-Edges	ATE (m) \downarrow	% Decrease \uparrow	Runtime (s) \downarrow	% real-time \downarrow
VBR <i>ciampino_train0</i>	DL Scale-Free	0.81 deg	0.36 deg	4513	1.53	83.65	711.64	45.94
	DL Absolute	0.25 m	0.48 deg	3338	1.81	80.70	1,600.84	103.35
	DL Both	/	/	6965	1.18	87.38	1,638.23	105.76
	MA Scale-Free	0.81 deg	0.39 deg	1389	2.02	78.48	1,427.77	92.17
	MA Absolute	1.96 m	2.50 deg	3402	3.92	58.14	1,419.91	91.67
	MA Both	/	/	3455	3.37	64.00	1,447.10	93.42
KITTI-00	DL Scale-Free	0.65 deg	0.17 deg	1547	6.87	47.44	235.54	50.16
	DL Absolute	0.77 m	0.99 deg	385	12.66	3.13	550.56	117.25
	DL Both	/	/	2164	1.70	86.98	571.10	121.63
	MA Scale-Free	0.79 deg	0.33 deg	448	14.73	-12.68	330.26	70.34
	MA Absolute	6.56 m	1.00 deg	562	3.79	70.98	342.97	73.04
	MA Both	/	/	587	3.71	71.58	349.61	74.46

TABLE I: **Performance comparison of different variants and LC-edge combinations of 2GO** KISS-ICP odometry is used for the *ciampino_train0* VBR sequence, with RMSE ATE: 9.37 m. Real-time duration: 1549.0 s. VINS-Fusion odometry is used for KITTI-00, with RMSE ATE: 13.07 m. real-time duration: 469.54 s

Variant	VINS-Fusion	VINS-PGO	ORB-SLAM3	Maplab-BIN	Maplab-SP	Kimera	2GO (Ours)
Runtime	1564 s	6206 s	1755 s	110 s (Map) 29 s (Opt)	14139 s (Map) 271 s (Opt)	1653 s	1167 s
Map Size	/	/	319 MB ₁ -28.8 GB	319 MB	572 MB	/	146 MB

TABLE II: **Comparison of runtime and map size** Result is across different methods for the *spagna_train0* trajectory of VBR (1414s real-time duration). “Maplab-BIN” and “Maplab-SP” denote Maplab pipeline using Binary feature with nearest neighbor matcher and SuperPoint feature with SuperGlue matcher.

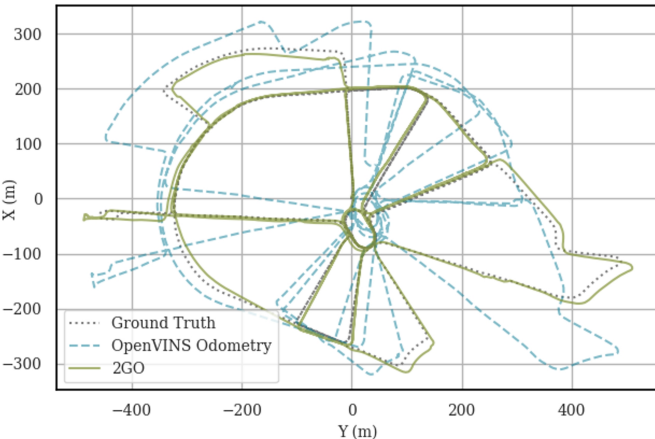


Fig. 4: **Trajectories of *ciampino_train0* sequence** 2GO improves upon the OpenVINS odometry input.

over the input trajectory, suggesting that this effect is linked to the trajectory scale. On certain sequences, 2GO provides only marginal improvement when using ORB-SLAM3 as the input odometry, sometimes achieving similar accuracy. In addition to the extreme local deviations mentioned earlier, this is primarily because some sequences are relatively short with limited visual overlap, where ORB-SLAM3 already performs well.

Figure 4 and Figure 5 present qualitative results. Despite the lack of global consistency in the OpenVINS input, 2GO effectively refines it, reducing ATE from 75.29 to 10.69. Leveraging vision priors and system adaptations, 2GO reliably constructs loop-closure edges from image pairs with significantly different viewpoints. These loop closures play a crucial role in improving global consistency. Additional results are provided in Appendix Section A.

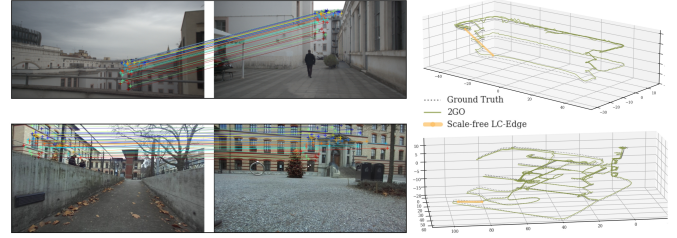


Fig. 5: **Scale-free LC Edge Examples** The top row contains samples from *diag_train0*, while the bottom row is from our real-world recording. Both LCs are constructed from very variant image baselines and contribute to trajectory refinement in the PGO.

E. Can 2GO improve further on good odometry?

While 2GO is designed for visual SLAM, it can also operate in a sensor-fusion setup using odometry input from other modalities, such as LiDAR. This enables us to assess whether trajectory improvements saturate with more accurate odometry sources. We tested this by using LiDAR odometry as input, with results presented in the rightmost section of Table III. 2GO improves the odometry input across all sequences, except for the short KITTI-07, demonstrating its applicability in a multi-modal sensor setup. This aligns with our initial hypothesis that 2GO can globally optimize an already robust odometry source. The results further confirm that our approach achieves better overall trajectory accuracy than prior visual SLAM methods.

F. How does 2GO work on a real-world robot?

We access the accuracy, scalability and real-world applicability of 2GO with a 1.1 hour, 2.7 km data recording on a Boston Dynamics Spot robot. The trajectory primarily covers different areas of a multi-floor building and a short outdoor segment, as shown in Figure 1. A Stereolabs Zed 2 camera provides images, IMU, and on-device VIO. Spot also provides device odometry, fused from leg and visual sources. To keep the size of the recorded data manageable, we performed 2GO’s keyframing online to spatio-temporally downsample the input image stream. In addition, input images were compressed before being saved to disk. The Zed and Spot odometries and IMU measurements were not downsampled. We use the pipeline of [67] to generate ground truth poses.

Sequence	Length	Duration	Visual Odometry			w/ VINS-Fusion			w/ ORB-SLAM3			w/ KISS-ICP		
			VINS-Fusion	OpenVINS	DPVO*	VINS-PGO	Kimera	Maplab-BIN	Maplab-SP	2GO	ORB-SLAM3	2GO	KISS-ICP	2GO
KITTI-00	3.72 km	470 s	13.09	no imu	113.17	4.20	no imu	11.13	11.39	1.58	4.85	4.67	3.97	1.30
KITTI-01	2.45 km	114 s	7.95	no imu	12.31	7.98	no imu	66.31	20.92	7.93	13.62	10.87	20.46	5.69
KITTI-02	5.07 km	483 s	21.02	no imu	123.21	13.02	no imu	23.96	18.29	10.58	5.64	6.88	6.94	3.46
KITTI-03	0.56 km	83 s	1.64	no imu	1.99	1.55	no imu	4.04	4.31	1.17	1.38	1.17	0.86	0.53
KITTI-04	0.39 km	28 s	1.30	no imu	0.83	1.25	no imu	2.27	2.47	1.31	0.34	0.38	0.44	0.30
KITTI-05	2.21 km	288 s	6.39	no imu	74.17	3.68	no imu	11.37	11.21	1.67	0.95	0.94	1.79	0.72
KITTI-06	1.23 km	114 s	3.54	no imu	76.72	1.68	no imu	13.27	14.76	1.48	0.79	0.71	0.91	0.53
KITTI-07	0.69 km	114 s	2.11	no imu	23.28	0.65	no imu	7.48	7.70	0.43	0.50	0.48	0.36	0.41
KITTI-08	3.22 km	423 s	10.43	no imu	135.46	10.01	no imu	17.04	14.27	3.79	3.67	3.78	4.06	3.35
KITTI-09	1.71 km	165 s	7.80	no imu	106.20	7.71	no imu	15.97	12.31	4.79	3.22	1.85	1.69	1.42
KITTI-10	0.92 km	125 s	3.77	no imu	25.55	3.73	no imu	9.17	9.46	1.56	1.19	1.03	1.95	1.47
campus_train0	2.73 km	602 s	lost 213s	32.53	69.57	vio failed	ov 26.04	ov 36.56	ov 33.40	ov 9.17	11.94	11.22	1.32	1.02
campus_train1	2.95 km	584 s	lost 197s	46.38	53.20	vio failed	vio failed	ov 47.77	ov 47.74	ov 23.03	7.99	7.72	3.44	0.53
ciampino_train0	9.01 km	1549 s	lost 32s	75.29	97.80	vio failed	ov 20.77	ov 61.55	ov 68.29	ov 10.69	68.11	71.04	22.82	1.27
ciampino_train1	5.20 km	942 s	lost 15s	39.17	111.25	vio failed	ov 6.75	ov 43.17	ov 42.80	ov 11.63	13.83	12.80	13.82	0.61
colosseo_train0	1.45 km	882 s	lost 13s	lost 518s	63.61	vio failed	vio failed	vio failed	vio failed	vio failed	9.67	8.98	4.79	0.34
diag_train0	1.04 km	1003 s	lost 335s	lost 453s	35.70	vio failed	vio failed	vio failed	vio failed	vio failed	29.06	31.35	4.02	0.58
pincio_train0	1.28 km	1114 s	63.02	lost 832s	75.40	48.03	147.79	74.80	99.54	19.97	2.08	1.11	1.61	0.66
spagna_train0	1.56 km	1414 s	183.28	lost 812s	54.94	183.42	275.74	275.52	335.46	250.58	5.62	4.10	2.86	0.48

TABLE III: RMSE ATE (m) after 6-DOF trajectory alignment. *Italic* indicates up-to-scale methods where scale alignment is also performed. “Lost” denotes loss of tracking. The best method for each odometry source is underlined, while the best non-LiDAR method is **bolded**. ^{ov} marks cases where OpenVINS replaces VINS-Fusion, which fails on the trajectory. VINS-Fusion is used as raw odometry without place recognition or PGO. On KITTI, it runs as stereo odometry due to the absence of IMU data, while on VBR, we use its VIO variant. ORB-SLAM3 is run in stereo-only mode. It tightly integrates its visual odometry and global optimization, making direct comparisons difficult. To address this, we use its output trajectory as pseudo-odometry for 2GO. Kimera requires its internal VIO, restricting evaluation to IMU-equipped datasets. To ensure fair comparison, we use the same external odometry source as 2GO and minimize the internal VIO’s impact by setting the external odometry fusion weight to 10 million, as recommended by the author of [20].

	Spot Odom	ZED Odom	ZED w/ LC	Maplab-BIN	Maplab-SP	2GO
RMSE ATE (m)	2.44	26.18	23.05	30.13	16.60	0.66
Runtime (s)	/	/	/	11 (Map) 21 (Opt)	4520 (Map) 85 (Opt)	902
Map Size (MB)	/	/	/	64.3	116.4	162.5

TABLE IV: **Comparison of mapping methods on a real-world trajectory** Maplab and 2GO use Spot Odom as an odometry input.

The aggressive keyframing required for the recording means that we cannot run visual odometry offline on the data. We therefore compare with the two available on-device odometries from the ZED and Spot, and with Maplab, which is the only baseline able to accept external odometry as its sole input source. Our results confirm that 2GO can be readily deployed on existing platforms using their provided odometry. It consistently operates within real-time constraints while maintaining a low-memory footprint for the map. Both Maplab variants produce notably small maps in this experiment. This is primarily due to the limited density of 3D landmarks that Maplab can generate, constrained by keyframing, large texture-poor regions in the scene, and high motion blur in some images. For comparison, in *spagna_train0* from VBR, the average number of 3D landmarks per keyframe is **20.17 (Binary)** and **82.25 (SuperPoint)**, whereas in this real-world sequence, it drops to **1.35** and **1.95**, respectively. This also helps explain Maplab’s lower performance.

VI. LIMITATIONS

Firstly, 2GO is a trajectory refinement method and thus requires an odometry source with high local precision. Currently, it cannot refine trajectories with discontinuities or scale errors. To handle such cases or support multi-session settings, 2GO’s proximity-based LC candidate selection and geometric

feasibility checks would need to be enhanced with additional methods.

Secondly, since 2GO relies on PGO for trajectory refinement, its runtime scales with the number of keyframes. Additionally, 2GO generates a large number of LC edges, making its pose graph denser than other PGO methods. Integrating complementary techniques for pose-graph sparsification [28, 29] could further improve scalability in this aspect.

VII. CONCLUSION

In this work, we presented 2GO, a novel approach to scalable visual SLAM that eliminates the need for dense scene reconstruction by leveraging two-view loop closures and monocular priors. By constraining the map to a sparse keyframed pose graph, we achieve a streamlined and computationally efficient optimization process while maintaining competitive trajectory accuracy. Our experiments on diverse datasets, including large-scale scenarios, highlight the effectiveness of recent advancements in image matching and monocular metric depth estimation for accurate trajectory estimation. The results demonstrate that 2GO enables real-time performance, scales effectively in both map size and trajectory duration, and is well-suited for long-duration deployments in large environments. This work broadens the scope of visual SLAM by offering a practical alternative for scenarios where dense reconstruction is unnecessary, paving the way for efficient and scalable solutions in autonomous navigation and mapping.

ACKNOWLEDGMENTS

We sincerely thank *Luca Di Giamarino* and *Simone Ferrari* from the Robots Vision and Perception Group at Sapienza

University of Rome for their assistance in obtaining ORB-SLAM3 results on VBR.

REFERENCES

[1] Ali Rida Sahili, Saifeldin Hassan, Saber Muawiyah Sakhrieh, Jinane Mounsef, Noel Maalouf, Bilal Arain, and Tarek Taha. A survey of visual slam methods. *IEEE Access*, 11:139643–139677, 2023.

[2] Cesar Cadena, Luca Carlone, Henry Carrillo, Yasir Latif, Davide Scaramuzza, José Neira, Ian D. Reid, and John J. Leonard. Simultaneous localization and mapping: Present, future, and the robust-perception age. *CoRR*, abs/1606.05830, 2016. URL <http://arxiv.org/abs/1606.05830>.

[3] Kamak Ebadi, Lukas Bernreiter, Harel Biggie, Gavin Catt, Yun Chang, Arghya Chatterjee, Christopher E Deniston, Simon-Pierre Deschênes, Kyle Harlow, Shehryar Khattak, et al. Present and future of slam in extreme environments: The darpa subt challenge. *IEEE Transactions on Robotics*, 2023.

[4] Julio A Placed, Jared Strader, Henry Carrillo, Nikolay Atanasov, Vadim Indelman, Luca Carlone, and José A Castellanos. A survey on active simultaneous localization and mapping: State of the art and new frontiers. *IEEE Transactions on Robotics*, 39(3):1686–1705, 2023.

[5] Marius Fehr, Thomas Schneider, and Roland Siegwart. Visual-inertial teach and repeat powered by google tango. In *2018 IEEE/RSJ International Conference on Intelligent Robots and Systems (IROS)*, pages 1–9. IEEE, 2018.

[6] Abdelrhman Werby, Chenguang Huang, Martin Büchner, Abhinav Valada, and Wolfram Burgard. Hierarchical open-vocabulary 3d scene graphs for language-grounded robot navigation. In *First Workshop on Vision-Language Models for Navigation and Manipulation at ICRA 2024*, 2024.

[7] Jiaqi Chen, Boyang Sun, Marc Pollefeys, and Hermann Blum. A 3d mixed reality interface for human-robot teaming. In *2024 IEEE International Conference on Robotics and Automation (ICRA)*, pages 11327–11333. IEEE, 2024.

[8] Christyan Cruz Ulloa, Jaime del Cerro, and Antonio Barrientos. Mixed-reality for quadruped-robotic guidance in sar tasks. *Journal of Computational Design and Engineering*, 10(4):1479–1489, 2023.

[9] Leiv Andresen, Adrian Brandemuehl, Alex Honger, Benson Kuan, Niclas Vödisch, Hermann Blum, Victor Reijgwart, Lukas Bernreiter, Lukas Schaupp, Jen Jen Chung, et al. Accurate mapping and planning for autonomous racing. In *2020 IEEE/RSJ international conference on intelligent robots and systems (IROS)*, pages 4743–4749. IEEE, 2020.

[10] Lukas Schaupp, Patrick Pfreundschuh, Mathias Bürki, Cesar Cadena, Roland Siegwart, and Juan Nieto. Mozard: Multi-modal localization for autonomous vehicles in urban outdoor environments. In *2020 IEEE/RSJ International Conference on Intelligent Robots and Systems (IROS)*, pages 4828–4833. IEEE, 2020.

[11] Gilad Baruch, Zhuoyuan Chen, Afshin Dehghan, Tal Dimry, Yuri Feigin, Peter Fu, Thomas Gebauer, Brandon Joffe, Daniel Kurz, Arik Schwartz, et al. Arkitscenes: A diverse real-world dataset for 3d indoor scene understanding using mobile rgb-d data. *arXiv preprint arXiv:2111.08897*, 2021.

[12] Tomáš Rouček, Martin Pecka, Petr Čížek, Tomáš Petříček, Jan Bayer, Vojtěch Šalanský, Daniel Heřt, Matěj Petrlík, Tomáš Báča, Vojtěch Spurný, François Pomerleau, Vladimír Kubelka, Jan Faigl, Karel Zimmermann, Martin Saska, Tomáš Svoboda, and Tomáš Krajiník. Darpa subterranean challenge: Multi-robotic exploration of underground environments. In *Modelling and Simulation for Autonomous Systems: 6th International Conference, MESAS 2019, Palermo, Italy, October 29–31, 2019, Revised Selected Papers*, page 274–290, Berlin, Heidelberg, 2019. Springer-Verlag. ISBN 978-3-030-43889-0. doi: 10.1007/978-3-030-43890-6_22. URL https://doi.org/10.1007/978-3-030-43890-6_22.

[13] Michael Helmberger, Kristian Morin, Beda Berner, Nitish Kumar, Giovanni Cioffi, and Davide Scaramuzza. The hilti slam challenge dataset. *IEEE Robotics and Automation Letters*, 7(3):7518–7525, 2022.

[14] Igor Cvišić, Ivan Marković, and Ivan Petrović. Soft2: Stereo visual odometry for road vehicles based on a point-to-epipolar-line metric. *IEEE Transactions on Robotics*, 39(1):273–288, 2022.

[15] Tong Qin, Peiliang Li, and Shaojie Shen. Vins-mono: A robust and versatile monocular visual-inertial state estimator. *IEEE Transactions on Robotics*, 34(4):1004–1020, August 2018. ISSN 1941-0468. doi: 10.1109/tro.2018.2853729. URL <http://dx.doi.org/10.1109/TRO.2018.2853729>.

[16] Stefan Leutenegger. Okvis2: Realtime scalable visual-inertial slam with loop closure, 2022. URL <https://arxiv.org/abs/2202.09199>.

[17] Zachary Teed, Lahav Lipson, and Jia Deng. Deep patch visual odometry. *Advances in Neural Information Processing Systems*, 2023.

[18] Sameer Agarwal, Noah Snavely, Steven M Seitz, and Richard Szeliski. Bundle adjustment in the large. In *Computer Vision–ECCV 2010: 11th European Conference on Computer Vision, Heraklion, Crete, Greece, September 5–11, 2010, Proceedings, Part II 11*, pages 29–42. Springer, 2010.

[19] Andrei Cramariuc, Lukas Bernreiter, Florian Tschopp, Marius Fehr, Victor Reijgwart, Juan Nieto, Roland Siegwart, and Cesar Cadena. maplab 2.0 – a modular and multi-modal mapping framework. *IEEE Robotics and Automation Letters*, 8(2):520–527, February 2023. ISSN 2377-3774. doi: 10.1109/lra.2022.3227865. URL <http://dx.doi.org/10.1109/LRA.2022.3227865>.

[20] Antoni Rosinol, Marcus Abate, Yun Chang, and Luca Carlone. Kimera: an open-source library for real-time

metric-semantic localization and mapping. In *2020 IEEE International Conference on Robotics and Automation (ICRA)*, pages 1689–1696. IEEE, 2020.

[21] Mu Hu, Wei Yin, Chi Zhang, Zhipeng Cai, Xiaoxiao Long, Hao Chen, Kaixuan Wang, Gang Yu, Chunhua Shen, and Shaojie Shen. Metric3d v2: A versatile monocular geometric foundation model for zero-shot metric depth and surface normal estimation. *arXiv preprint arXiv:2404.15506*, 2024.

[22] Vincent Leroy, Yohann Cabon, and Jerome Revaud. Grounding image matching in 3d with mast3r, 2024.

[23] Tong Qin, Shaozu Cao, Jie Pan, and Shaojie Shen. A general optimization-based framework for global pose estimation with multiple sensors, 2019.

[24] Carlos Campos, Richard Elvira, Juan J Gómez Rodríguez, José MM Montiel, and Juan D Tardós. Orb-slam3: An accurate open-source library for visual, visual-inertial, and multimap slam. *IEEE Transactions on Robotics*, 37(6):1874–1890, 2021.

[25] Andreas Geiger, Philip Lenz, and Raquel Urtasun. Are we ready for autonomous driving? the kitti vision benchmark suite. In *Conference on Computer Vision and Pattern Recognition (CVPR)*, 2012.

[26] Michael Burri, Janosch Nikolic, Pascal Gohl, Thomas Schneider, Joern Rehder, Sammy Omari, Markus W Achtelik, and Roland Siegwart. The euroc micro aerial vehicle datasets. *The International Journal of Robotics Research*, 2016. doi: 10.1177/0278364915620033. URL <http://ijr.sagepub.com/content/early/2016/01/21/0278364915620033.abstract>.

[27] Stefan Leutenegger, Paul Furgale, Vincent Rabaud, Margarita Chli, Kurt Konolige, and Roland Siegwart. Keyframe-based visual-inertial slam using nonlinear optimization. *Proceedings of Robotis Science and Systems (RSS) 2013*, 2013.

[28] Viorela Ila, Josep M Porta, and Juan Andrade-Cetto. Information-based compact pose slam. *IEEE Transactions on Robotics*, 26(1):78–93, 2009.

[29] Hordur Johannsson, Michael Kaess, Maurice Fallon, and John J Leonard. Temporally scalable visual slam using a reduced pose graph. In *2013 IEEE International Conference on Robotics and Automation*, pages 54–61. IEEE, 2013.

[30] Richard A Newcombe, Steven J Lovegrove, and Andrew J Davison. Dtam: Dense tracking and mapping in real-time. In *2011 international conference on computer vision*, pages 2320–2327. IEEE, 2011.

[31] Zihan Zhu, Songyou Peng, Viktor Larsson, Zhaopeng Cui, Martin R Oswald, Andreas Geiger, and Marc Pollefeys. Nicer-slam: Neural implicit scene encoding for rgb slam. In *International Conference on 3D Vision (3DV)*, March 2024.

[32] Wei Yin, Chi Zhang, Hao Chen, Zhipeng Cai, Gang Yu, Kaixuan Wang, Xiaozhi Chen, and Chunhua Shen. Metric3d: Towards zero-shot metric 3d prediction from a single image. In *Proceedings of the IEEE/CVF International Conference on Computer Vision*, pages 9043–9053, 2023.

[33] Lihe Yang, Bingyi Kang, Zilong Huang, Zhen Zhao, Xiaogang Xu, Jiashi Feng, and Hengshuang Zhao. Depth anything v2. *arXiv:2406.09414*, 2024.

[34] Paul-Edouard Sarlin, Daniel DeTone, Tomasz Malisiewicz, and Andrew Rabinovich. SuperGlue: Learning feature matching with graph neural networks. In *CVPR*, 2020. URL <https://arxiv.org/abs/1911.11763>.

[35] Johan Edstedt, Qiyu Sun, Georg Bökmä, Mårten Wadenbäck, and Michael Felsberg. RoMa: Robust Dense Feature Matching. *IEEE Conference on Computer Vision and Pattern Recognition*, 2024.

[36] Jiaming Sun, Zehong Shen, Yuang Wang, Hujun Bao, and Xiaowei Zhou. Loftr: Detector-free local feature matching with transformers. In *Proceedings of the IEEE/CVF conference on computer vision and pattern recognition*, pages 8922–8931, 2021.

[37] Relja Arandjelovic, Petr Gronát, Akihiko Torii, Tomás Pajdla, and Josef Sivic. Netvlad: CNN architecture for weakly supervised place recognition. *Corr*, abs/1511.07247, 2015. URL <http://arxiv.org/abs/1511.07247>.

[38] Nikhil Keetha, Avneesh Mishra, Jay Karhade, Krishna Murthy Jatavallabhula, Sebastian Scherer, Madhava Krishna, and Sourav Garg. Anyloc: Towards universal visual place recognition. *IEEE Robotics and Automation Letters*, 9(2):1286–1293, 2023. doi: 10.1109/LRA.2023.3343602.

[39] Shuzhe Wang, Vincent Leroy, Yohann Cabon, Boris Chidlovskii, and Jerome Revaud. Dust3r: Geometric 3d vision made easy. In *CVPR*, 2024.

[40] Paul-Edouard Sarlin, Cesar Cadena, Roland Siegwart, and Marcin Dymczyk. From coarse to fine: Robust hierarchical localization at large scale. In *CVPR*, 2019.

[41] Eduardo Arnold, Jamie Wynn, Sara Vicente, Guillermo Garcia-Hernando, Áron Monszpart, Victor Adrian Prisacariu, Daniyar Turmukhambetov, and Eric Brachmann. Map-free visual relocalization: Metric pose relative to a single image. In *ECCV*, 2022.

[42] Axel Barroso-Laguna, Sowmya Munukutla, Victor Prisacariu, and Eric Brachmann. Matching 2d images in 3d: Metric relative pose from metric correspondences. In *CVPR*, 2024.

[43] Albert Gassol Puigjaner, Irvin Aloise, and Patrik Schmuck. Augmented reality without borders: Achieving precise localization without maps, 2024. URL <https://arxiv.org/abs/2408.17373>.

[44] Bardienus Duisterhof, Lojze Zust, Philippe Weinzaepfel, Vincent Leroy, Yohann Cabon, and Jerome Revaud. Mast3r-sfm: a fully-integrated solution for unconstrained structure-from-motion. *arXiv preprint arXiv:2409.19152*, 2024.

[45] Jianing Yang, Alexander Sax, Kevin J Liang, Mikael Henaff, Hao Tang, Ang Cao, Joyce Chai, Franziska Meier, and Matt Feiszli. Fast3r: Towards 3d reconstruc-

tion of 1000+ images in one forward pass. *arXiv preprint arXiv:2501.13928*, 2025.

[46] Riku Murai, Eric Dexheimer, and Andrew J. Davison. MAST3R-SLAM: Real-time dense SLAM with 3D reconstruction priors. *arXiv preprint*, 2024.

[47] Amar Ali-bey, Brahim Chaib-draa, and Philippe Giguère. BoQ: A place is worth a bag of learnable queries. In *Proceedings of the IEEE/CVF Conference on Computer Vision and Pattern Recognition (CVPR)*, pages 17794–17803, June 2024.

[48] Titus Cieslewski, Siddharth Choudhary, and Davide Scaramuzza. Data-efficient decentralized visual slam. In *2018 IEEE international conference on robotics and automation (ICRA)*, pages 2466–2473. IEEE, 2018.

[49] Philipp Lindenberger, Paul-Edouard Sarlin, and Marc Pollefeys. LightGlue: Local Feature Matching at Light Speed. In *ICCV*, 2023.

[50] Michał Tyszkiewicz, Pascal Fua, and Eduard Trulls. Disk: Learning local features with policy gradient. *Advances in Neural Information Processing Systems*, 33, 2020.

[51] Richard Hartley and Andrew Zisserman. *Multiple View Geometry in Computer Vision*. Cambridge University Press, New York, NY, USA, 2 edition, 2003. ISBN 0521540518.

[52] Matthew Boler and Scott Martin. Essential poseslam: An efficient landmark-free approach to visual-inertial navigation. In *2023 IEEE/ION Position, Location and Navigation Symposium (PLANS)*, pages 1341–1349, 2023. doi: 10.1109/PLANS53410.2023.10140080.

[53] Joan Solà, Jérémie Deray, and Dinesh Athchuthan. A micro lie theory for state estimation in robotics. *CoRR*, abs/1812.01537, 2018. URL <http://arxiv.org/abs/1812.01537>.

[54] Marcus Abate, Yun Chang, Nathan Hughes, and Luca Carlone. Kimera2: Robust and accurate metric-semantic slam in the real world, 2024. URL <https://arxiv.org/abs/2401.06323>.

[55] Johannes Lutz Schönberger and Jan-Michael Frahm. Structure-from-motion revisited. In *Conference on Computer Vision and Pattern Recognition (CVPR)*, 2016.

[56] Frank Dellaert and GTSAM Contributors. borglab/gtsam, May 2022. URL <https://github.com/borglab/gtsam>.

[57] Gim Hee Lee, Friedrich Fraundorfer, and Marc Pollefeys. Robust pose-graph loop-closures with expectation-maximization. In *2013 IEEE/RSJ International Conference on Intelligent Robots and Systems*, pages 556–563. IEEE, 2013.

[58] D. Schubert, T. Goll, N. Demmel, V. Usenko, J. Stueckler, and D. Cremers. The tum vi benchmark for evaluating visual-inertial odometry. In *International Conference on Intelligent Robots and Systems (IROS)*, October 2018.

[59] Thomas Schöps, Torsten Sattler, and Marc Pollefeys. BAD SLAM: Bundle adjusted direct RGB-D SLAM. In *Conference on Computer Vision and Pattern Recognition (CVPR)*, 2019.

[60] Leonardo Brizi, Emanuele Giacomini, Luca Di Giacomo, Simone Ferrari, Omar Salem, Lorenzo De Rebotti, and Giorgio Grisetti. Vbr: A vision benchmark in rome, 2024. URL <https://arxiv.org/abs/2404.11322>.

[61] Patrick Geneva, Kevin Eckenhoff, Woosik Lee, Yulin Yang, and Guoquan Paul Huang. Openvins: A research platform for visual-inertial estimation. 2020 *IEEE International Conference on Robotics and Automation (ICRA)*, pages 4666–4672, 2020. URL <https://api.semanticscholar.org/CorpusID:204745914>.

[62] Ignacio Vizzo, Tiziano Guadagnino, Benedikt Mersch, Louis Wiesmann, Jens Behley, and Cyrill Stachniss. KISS-ICP: In Defense of Point-to-Point ICP – Simple, Accurate, and Robust Registration If Done the Right Way. *IEEE Robotics and Automation Letters (RA-L)*, 8(2):1029–1036, 2023. doi: 10.1109/LRA.2023.3236571.

[63] Heng Yang, Pasquale Antonante, Vasileios Tzoumas, and Luca Carlone. Graduated non-convexity for robust spatial perception: From non-minimal solvers to global outlier rejection. *CoRR*, abs/1909.08605, 2019. URL <http://arxiv.org/abs/1909.08605>.

[64] Daniel DeTone, Tomasz Malisiewicz, and Andrew Rabenovich. Superpoint: Self-supervised interest point detection and description. *CoRR*, abs/1712.07629, 2017. URL <http://arxiv.org/abs/1712.07629>.

[65] Michael Grupp. evo: Python package for the evaluation of odometry and slam. <https://github.com/MichaelGrupp/evo>, 2017.

[66] S. Umeyama. Least-squares estimation of transformation parameters between two point patterns. *IEEE Transactions on Pattern Analysis and Machine Intelligence*, 13(4):376–380, 1991. doi: 10.1109/34.88573.

[67] Paul-Edouard Sarlin, Mihai Dusmanu, Johannes L. Schönberger, Pablo Speciale, Lukas Gruber, Viktor Larsson, Ondrej Miksik, and Marc Pollefeys. LaMAR: Benchmarking Localization and Mapping for Augmented Reality. In *ECCV*, 2022.

APPENDIX A TRAJECTORY VISUALIZATION

We visualize KITTI trajectories in Figure 6 and VBR trajectories in Figures 7, 8, 9, 10, and 11.

APPENDIX B CUMULATIVE TIMING

The following section breaks down the time required for 2GO’s different components over illustrative sequences in VBR. All illustrated sequences are running the DL variant with both scale-free and absolute LC-Edges.

Figure 12a and Figure 12b show typical examples of the runtime of 2GO. The computation time is dominated by image matching and relative pose estimation. However, as the input size increases, the time needed for PGO also increases significantly.

Figure 13a shows how runtime may be affected in environments where image retrieval yields many candidate LC-Edges. The overall runtime for this sequence could have been lowered by reducing the number of LC-Edges retrieved. An inverse example is in Figure 13b, where there are comparatively fewer LC-Edges retrieved, and the overall runtime is thus much lower.

APPENDIX C HYPERPARAMETERS

A full list of hyperparameters for each experimental configuration is enumerated in Table V. Below, each parameter is listed along with its effect.

- 1) δ_t^{KF} : Threshold for selecting current image as keyframe based on its distance to prev keyframe in meters.
- 2) δ_r^{KF} : Threshold for selecting current image as keyframe based on its angle to prev keyframe in radians.
- 3) M_F : Minimum similarity score between global descriptors $\langle \mathbf{F}_k, \mathbf{F}_a \rangle$ for \mathcal{I}_a to be considered a similarity LC.
- 4) N_{sim} : Number of similarity LCs to retrieve.
- 5) N_{prox} : Number of proximity LCs to retrieve.
- 6) M_{baseline} : Minimum distance between LC candidate and current keyframe in $\hat{\mathcal{X}}$.
- 7) $M_{\delta r}$: Maximum angle between LC candidate and current keyframe in $\hat{\mathcal{X}}$ in degrees.
- 8) $M_{\Delta t}$: Minimum time difference between LC candidate and current keyframe.
- 9) δ_t : Maximum distance in meters between LC candidate and current keyframe for a proximity LC to be considered, as described in Equation (2).
- 10) δ_r : Maximum angle in degrees between LC candidate and current keyframe for a proximity LC to be considered, as described in Equation (2).
- 11) $M_{\text{2D-2D}}$: Minimum number of 2D-2D matches that fit a geometric model for relative pose estimation, as described in Section IV-C.
- 12) M_d : Maximum depth in meters of lifted keypoints from MDE / MAST3R. Lifted keypoints beyond this depth are not used for absolute LC-Edges.

- 13) $M_{\text{3D-2D}}$: Minimum number of 3D-2D matches that fit a geometric model in PnP, as described in Section IV-C.
- 14) $\sigma_{\mathcal{O},t}$: Weighting of the translation component of odometry edges in PGO in meters.
- 15) $\sigma_{\mathcal{O},r}$: Weighting of the rotation component of odometry edges in PGO in degrees.
- 16) $\sigma_{\mathcal{L}s,t}$: Weighting of the translation component of scale-free LC-Edges in meters.
- 17) $\sigma_{\mathcal{L}a,t}$: Weighting of the translation component of absolute LC-Edges in meters.
- 18) $\sigma_{\mathcal{L},r}$: Weighting of the rotation component of both scale-free and absolute LC-Edges in degrees.
- 19) $M_{r,ta}$: Maximum discrepancy in translation between estimated translation in absolute LC-Edge \mathbf{t}_a^k and the value in $\hat{\mathcal{X}}$ in meters.
- 20) $M_{r,ts}$: Maximum discrepancy in angle between unit vectors of estimated translation in absolute LC-Edge \mathbf{t}_a^k and the value in $\hat{\mathcal{X}}$ in degrees.
- 21) $M_{r,r}$: Maximum discrepancy in rotation between estimated relative rotation of LC-Edge \mathbf{R}_a^k and the value in $\hat{\mathcal{X}}$ in degrees.

Furthermore, l , which controls how often PGO is performed, is set at 5 for all experiments.

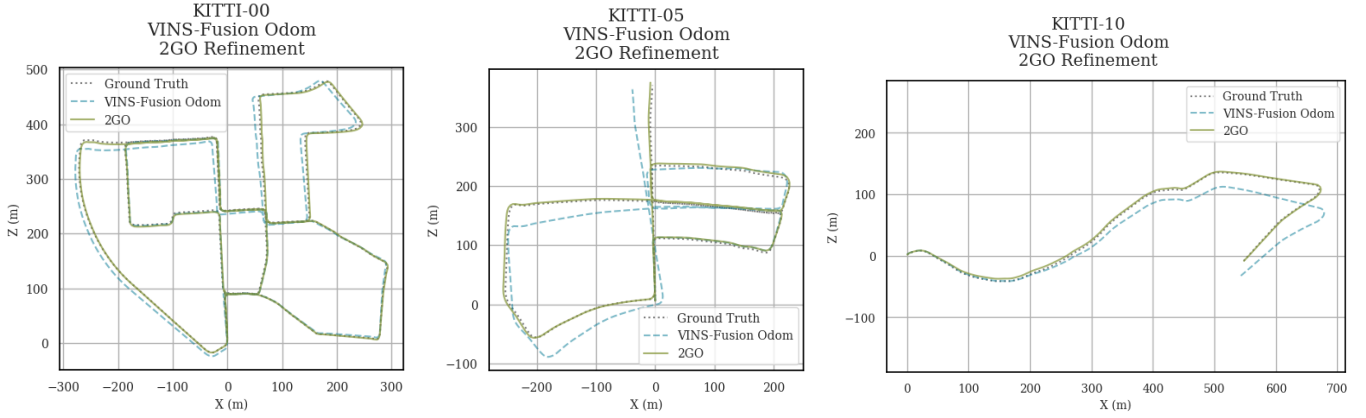


Fig. 6: Qualitative examples of 2GO refining VINS-Fusion odometry on various KITTI sequences. In particular, despite the limited opportunities for loop closure in KITTI-10, 2GO still manages to refine the odometry.

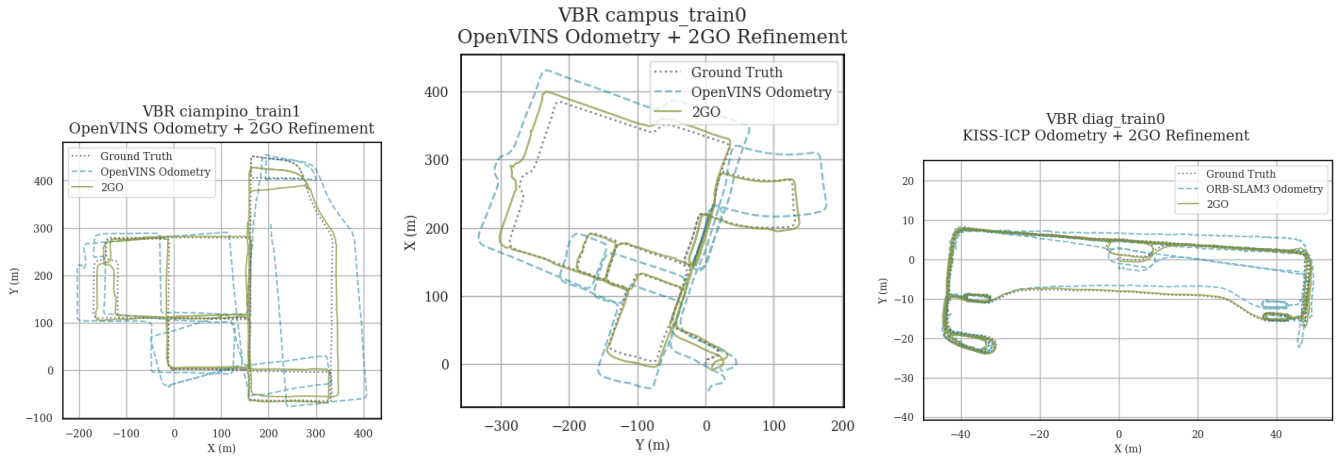


Fig. 7: Qualitative examples of 2GO significantly improving input odometry on various VBR sequences.

	δ_t^{KF}	δ_r^{KF}	M_F	N_{sim}	N_{prox}	M_{baseline}	$M_{\delta\tau}$	$M_{\Delta t}$	δ_t	δ_r	$M_{\text{2D-2D}}$	M_d	$M_{\text{3D-2D}}$	$\sigma_{\mathcal{O},r}$	$\sigma_{\mathcal{O},t}$	$\sigma_{\mathcal{Z},r}$	$\sigma_{\mathcal{Z},s,t}$	$\sigma_{\mathcal{Z},r}$	$M_{r,t}$	$M_{r,ts}$	$M_{r,r}$
KITTI VINS-Fusion	5.0	0.5	0.2	10	10	1.0	90.0	1.0	25.0	90.0	100	30.0	20	0.1	1.0	0.2	2.0	2.5	12.5	10.0	10.0
KITTI KISS-ICP	5.0	0.5	0.2	10	10	1.0	65.0	1.0	25.0	65.0	100	30.0	20	0.1	0.5	0.2	2.0	2.5	12.5	10.0	10.0
KITTI ORB-SLAM3	5.0	0.5	0.2	10	10	1.0	90.0	2.5	25.0	90.0	100	15.0	20	0.1	0.5	0.4	0.8	2.0	12.5	10.0	10.0
VBR Handheld OpenVINS	5.0	0.5	0.2	10	0	0.1	90.0	5.0	25.0	65.0	100	30.0	10	1.0	1.0	0.2	2.5	12.5	10.0	10.0	
VBR Handheld KISS-ICP	1.5	0.5	0.2	10	10	1.0	65.0	25.0	25.0	65.0	100	15.0	20	0.1	0.5	0.2	2.5	12.5	10.0	10.0	
VBR Handheld ORB-SLAM3	2.5	0.5	0.2	10	5	0.1	90.0	5.0	25.0	65.0	100	30.0	10	0.1	0.5	0.2	2.5	12.5	10.0	10.0	
VBR Vehicle VINS-Fusion	5.0	0.5	0.2	10	10	1.0	90.0	2.5	25.0	90.0	100	30.0	20	0.1	1.0	2.5	0.5	2.5	25.0	25.0	25.0
VBR Vehicle KISS-ICP	5.0	0.5	0.2	10	10	1.0	65.0	25.0	25.0	65.0	100	30.0	20	0.1	0.5	0.2	0.5	2.5	12.5	10.0	10.0
VBR Vehicle ORB-SLAM3	5.0	0.5	0.2	10	10	1.0	90.0	2.5	25.0	90.0	100	30.0	20	0.1	1.0	0.4	0.4	2.0	12.5	10.0	10.0
Real-World	2.0	1.0	0.2	10	10	0.1	65.0	2.5	15.0	45.0	200	15.0	20	0.1	0.5	0.2	1.0	2.5	5.0	7.5	7.5

TABLE V: List of parameters used in 2GO over all experiments.

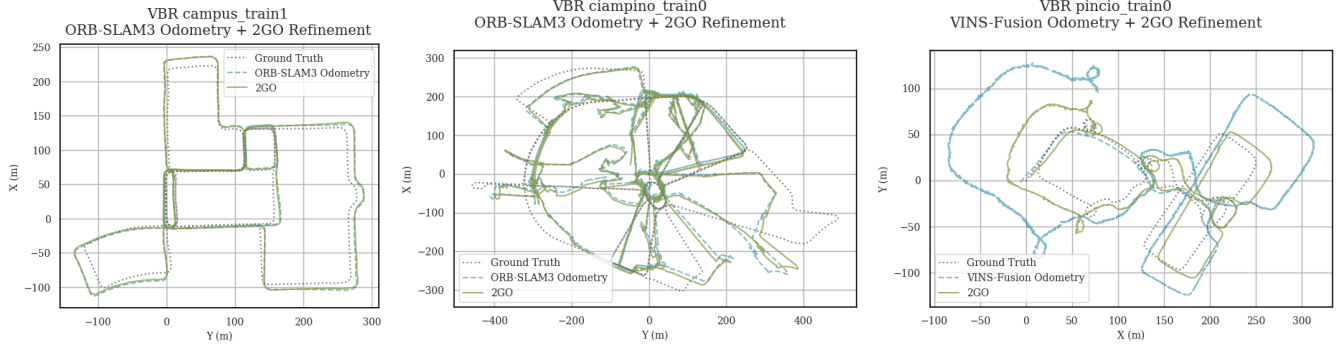


Fig. 8: Qualitative examples of 2GO struggling with bad trajectory inputs on various VBR sequences.

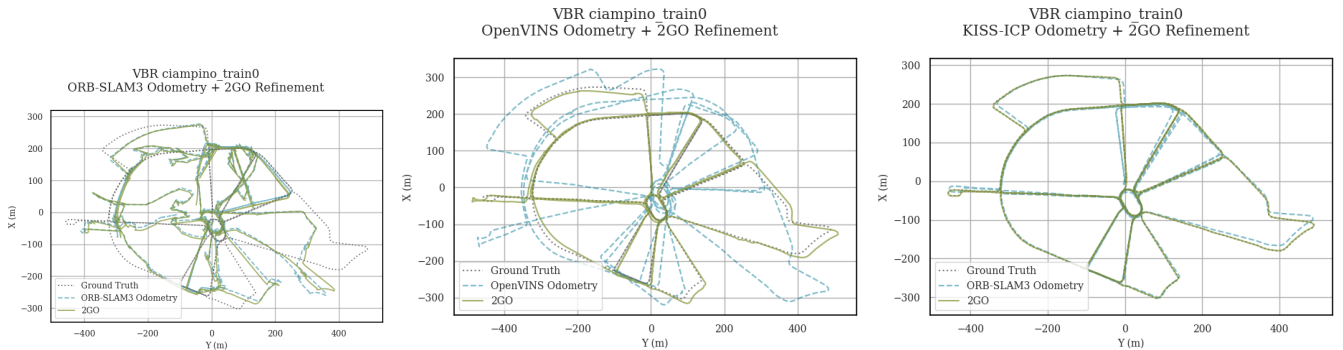


Fig. 9: Qualitative examples of 2GO on the *ciampino_train0* VBR sequence with various odometry inputs. Left to right: 2GO performs better with locally consistent input trajectories.

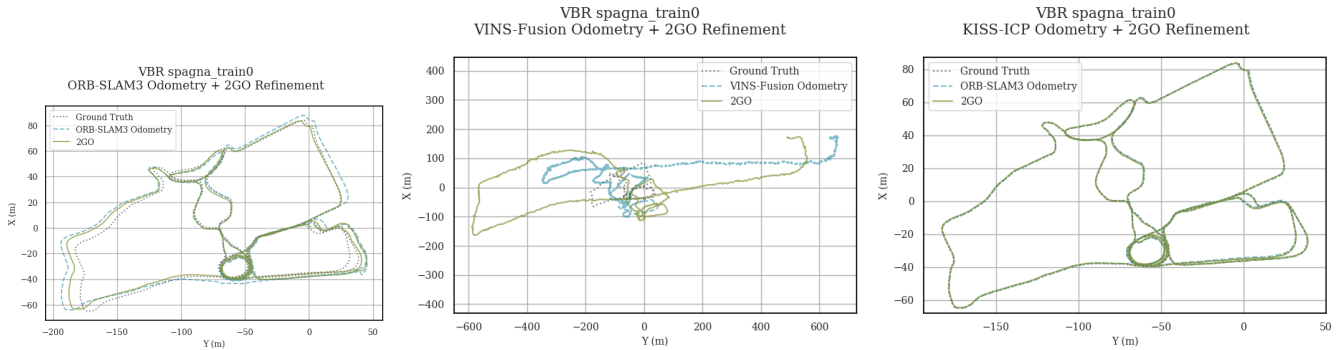


Fig. 10: Qualitative examples of 2GO on the *spagna_train0* VBR sequence with various odometry inputs, again illustrating how 2GO's performance varies on the quality of the input trajectory.

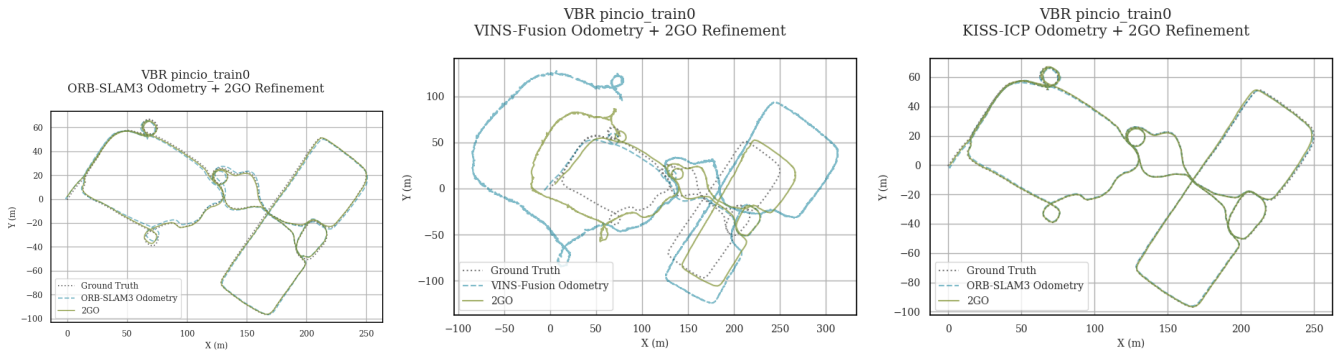
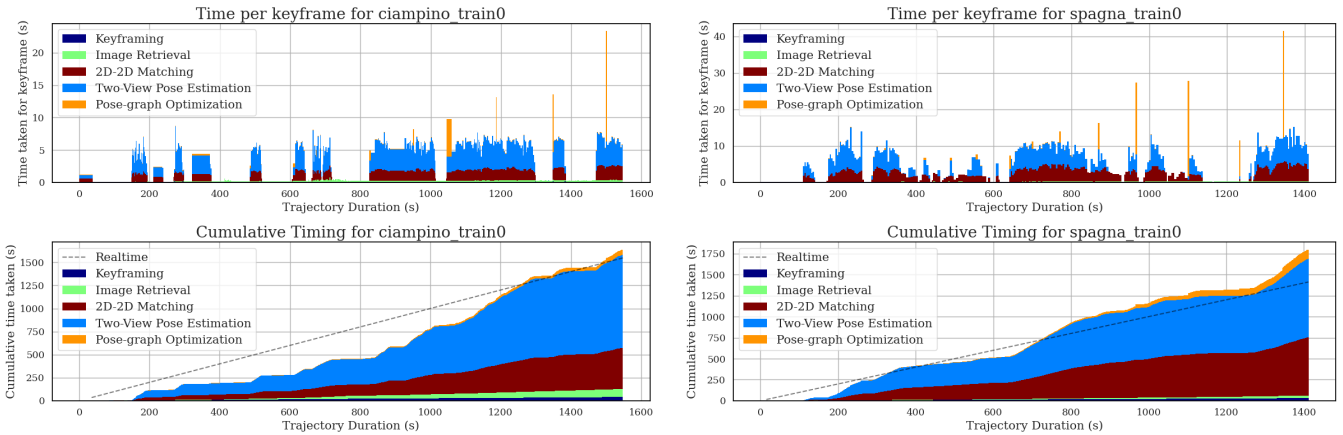
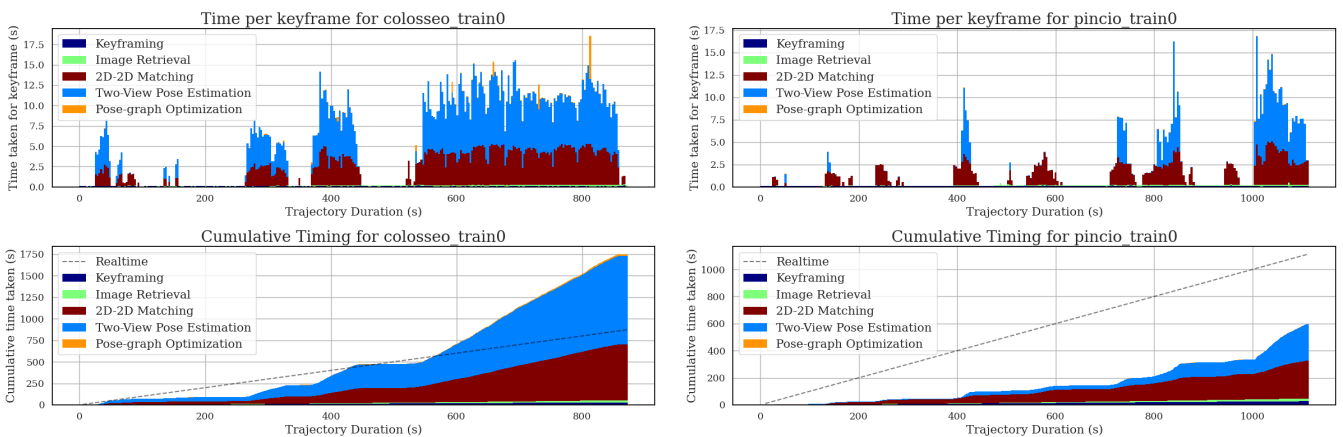


Fig. 11: Qualitative examples of 2GO on the *pincio_train0* VBR sequence with various odometry inputs.



(a) Cumulative timing for 2GO components on the *ciampino_train0* VBR sequence (b) Cumulative timing for 2GO components on the *spagna_train0* VBR sequence



(a) Cumulative timing for 2GO components on the *colosseo_train0* VBR sequence (b) Cumulative timing for 2GO components on the *pincio_train0* VBR sequence